北海道大学工学部研究報告
第130号（昭和61年）

Bulletin of the Faculty of Engineering,
Hokkaido University, No. 130 (1986)

The Growth Mechanism of Interfacial Wave Packet

Shizuo YOSHIDA*

(Received November 20, 1985)

Abstract

Using a flow visualization technique and an LDA system, the growth mechanism of interfacial wave packets is investigated at a small scale river mouth. Visual observation shows that the growth of the packet is closely connected with the intermittent instability of internal shear flow, and the intermittent results from the production of a localized high shear induced by a concentrated large-scale vortex intermittently occurring in the principal flow. These qualitative results are supported by the linear stability theory for a viscid two-layer flow.

1. Introduction

In the late period of the last century, the stability problem in statically stable two layer flow was treated by Helmholtz[1] and Kelvin[2] theoretically. Their results were investigated by Thorpe[3] through the experiments of exchange flows. His experiments which used the flow visualization technique show that the instability found theoretically by Helmholtz and Kelvin causes the generation of the spiral vortices of which the centers coincide with the interface. However, since the K-H flow model has an infinite velocity gradient at the interface, he could not confirm the K-H criterion on the actual inviscid flow instability. Instead, he found an agreement between his own experimental and theoretical results on wave growth rate for real velocity profiles. At present, however, we extend the definition of the K-H instability to the Thorpe's spiral vortices, and often call them the K-H instability or the K-H instability wave at a nonlinear stage.

Keulegan[4] examined experimentally the condition of an interfacial wave breaking when fresh water flows over the arrested saline water in a one dimensional horizontal channel. Without taking into consideration the flow instability, he introduced the dimensionless parameter called the Keulegan number for classifying the interfacial phenomena. However the interfacial wave he observed was different from the K-H instability in that it had an antisymmetric breaking structure in which the breaking of the wave crest occurs only in the principal flow layer. As a result of his experiments, it was predicted that there is another growth mechanism of the interfacial wave in addition to the K-H instability.

The existence of mechanisms different from the Thorpe type K-H instability had already been proved by Holmboe[5] before Thorpe's experimental work. He investigated the flow instability of inviscid two layer flows which had symmetric velocity and density profiles.

* Department of Engineering Science, Faculty of Engineering, Hokkaido University, Sapporo, Japan

The instability wave through this mechanism is considered to be the resultant wave after the composing of two waves of which the phase velocities are equal in magnitude but opposite in direction. Therefore, the Keulegan type wave breaking observed in the principal flow layer could not be predicted from his results. Hazel continued this work and went on to investigate the relation between the dimensionless parameter, the Richardson number, and their instability mechanisms. His numerical analysis was also based on the theory for the inviscid flow of symmetric velocity and density profiles. Therefore, it was impossible to obtain the criterion of the wave generation dependent on the Reynolds number and to explain the antisymmetric wave breaking only in the principal flow layer.

Yoshida[7),8)] carried out a series of experimental and theoretical investigations of the two layer flow with an antisymmetric velocity and density profile. He found the interfacial waves different from the Keulegan wave in an experiment of the selective withdrawal from a two-layered fluids system. The breaking structure of this wave and the Keulegan wave are symmetric with regard to the interface. The result suggests that the symmetric Holmboe waves are isolated in an antisymmetric flow. His work was further extended to the wave growth mechanism, and it was clarified that these waves are the interfacial deformations due to the spiral vortices growing just above and beneath the interface. The growing mechanism of the vortices has been investigated by subsequent authors experimentally[9)] as well as numerically.[10),11)]

In this paper, we show that the interfacial waves are generally observed as a wave packet, and then clarify the reason for it experimentally as well as theoretically. As a large scale vortex occurring in the principal flow layer plays an important part in explaining the phenomenon, our investigection is extended to the fine structure of the principal flow.

2. Experimental aparatus and Procedures

An experiment was carried out using an hydraulic model of a two-layer flow system at a rives mouth. In practice the saline-fresh water system was formed in the transparent rectangular channel of which one side opened into a wide reservoir as in Fig. 1. The test section was made of transparent plate glass to facilitate visualization. Uranin ($C_{20}H_{10}Na_2O_2$) was mostly used as a dye material. The dye method worked better in the flow system having a nonhomogeneous electrical conductivity than in the hydrogen bubble technique. Using a black light together with Uranin, visual observation was made quite successfully.

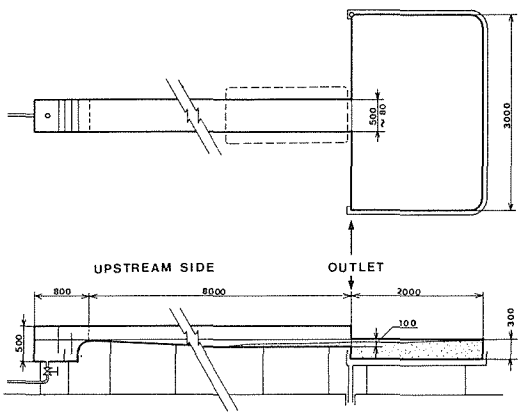

Fig. 1 Schematic drawing of test channel and accessories.

The velocity fluctuations were measured at four vertical points with a multichannel LDA shown in Fig. 2 so that a time evolution of velocity profile could be obtained. Whether the internal shear became high or not was judged from the data obtained by this method.

The interfacial wave heights were measured with an electrode probe. In order to obtain the output signals linear to the wave heights, we obtained an appropriate calibration curve. However, since we could obtain the essential data from the direct output signals, the procedure of the calibration was omitted.

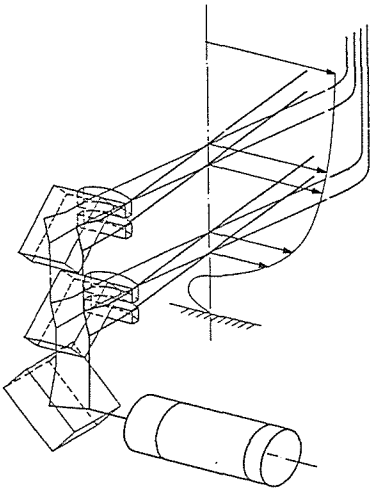

Fig. 2 Optical system for multichannel LDA.

3. Experimental results

There are three typical types of interfacial waves which grow at the interface of a miscible stratified flow system. These waves can be found independently in a model of a two-layer flow system at a river mouth. The illustration in Fig. 3 shows the flow model and the above three interfacial waves in schematic design. Figs. 4, 5, and 6 show the shapes of these waves and a streak line just above or beneath the interface. The pictures were taken by using a Uranin solution and a slit light beam. The streak lines near the interface indicate that each wave make a packet shape and is accompanied by a spiral vortex which has its own growing level to the interface. The spiral vortex which has a center just on the interface corresponds to Thorpe's spiral wave ; the author calls this vortex SVC. As the other two vortices appear in the shear layer just above and beneath the interface respectively, the author calls the former SVA (Fig. 5) and the latter SVB (Fig. 6). Each of these vortices has an individual phase velocity. Therefore, the phase velocities of the interfacial waves are equivalent to those of the vortices respectively. These waves appear in a restricted area as shown in Fig. 3 ; SVA, SVB, and SVC are observed at the interface of the lower layer front, the estuary near the mouth and the outlet offing, respectively. The Keulegan wave probably corresponds to SVA judging by the shape. If this fact is true, the wave breaking investigated

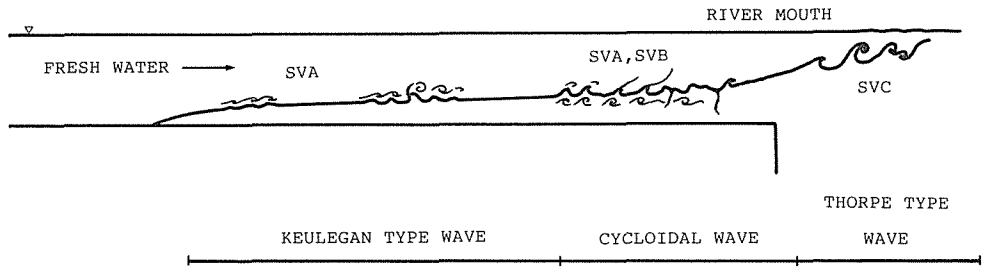

Fig. 3 Side view of the flow system and the interfacial phenomena.

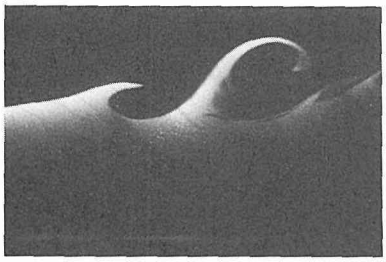

Fig. 4 Thorpe type wave or SVC.

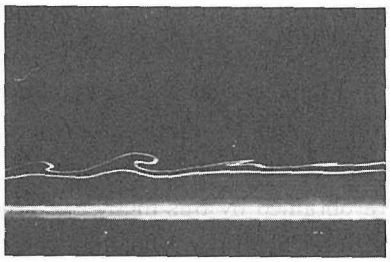

Fig. 5 Keulegan type wave and SVA.

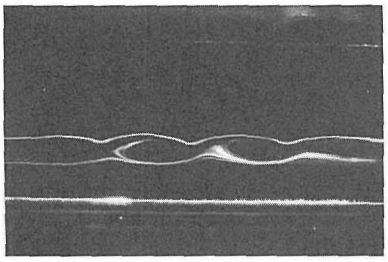

Fig. 6 Cycloidal wave and SVB.

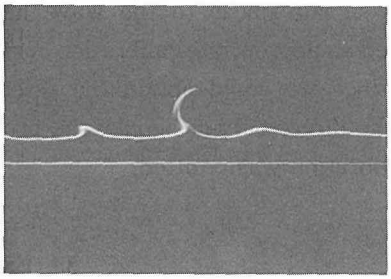

Fig. 7 Breaking stage of Keulegan type waves.

by Keulegan is based on an exceeding growth of SVA. In this case, the wave crest is entrained in the vortex core of SVA as shown in Fig. 7. This breaking stage is much like that of the Keulegan wave. It is also important to note the crest at this stage. The crest of the waves in the photograph are inclined in the opposite direction to the propagating direction of SVA. According to the water wave theory, the wave crest should incline toward in to the propagating direction of the wave at its nonlinear stage. This means that it is impossible to explain the phenomenon without considering the interaction between SVA and the interfacial wave.

As stated above the interfacial waves in a two-layer flow system usually have the shape of a wave packet. Through the visual observation, the qualitative growth mechanism of the wave packet is clarified as follows. The laminar longitudinal vortices which have axes in the direction of the mean flow generate as the flow velocity increases. Fig. 8 shows the cross sectional streak lines of this vortices. The longitudinal vortices force the appearance of the long-high speed zone and the long-low speed zone in the principal flow layer parallel with their axes. The interfacial waves generate first at the interface beneath the high speed zone (Fig. 9), and after that, their time evolution is also observed in the same zone. The longitudinal vortices each begin to meander with the increase of the mean velocity. Finally, the longitudinal vortex changes to the large scale vortex having a horizontal axis at almost right angles to the principal flow direction. The latter vortex is probably generated through the Rayleigh instability. Since the large scale vortex accelerates only the shear flow beneath it, a local high shear zone moving with the vortex is created near the interface. Thus, the preparation of the generation for the instability wave packet, i. e. SVA packet, has been completed. Although the generation of SVB packet is related in the case of lower layer, the qualitative mechanism resembles the SVA case. In order to conclude that the wave packets

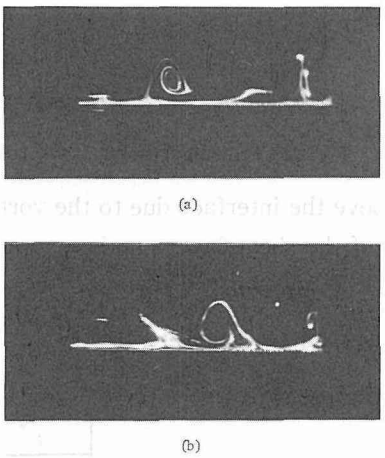

Fig. 8 Vertical and cross sectional flow pattern of longitudinal vortex. (a) clockwise spiral pattern. (b) Counter clockwise spiral pattern.

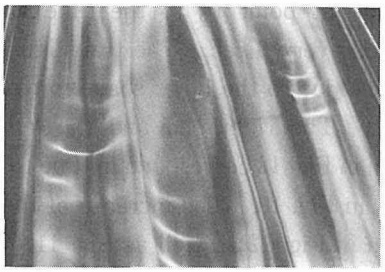

Fig. 9 Interfacial wave packets restricted with in narrow interfaces beneath the high speed flows induced by longitudinal vortices.

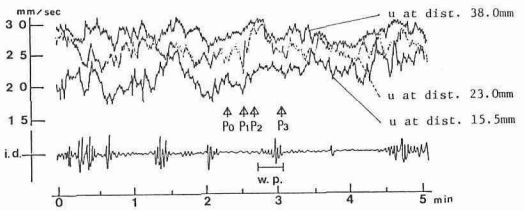

Fig. 10 Oscillograms of horizontal velocities measured by multichannel LDA and displacement of interface.

grow owing to the shear instability, we further confirmed it quantitatively.

Fig. 10 shows the velocities measured at three vertical points in the principal flow layer. The measuring position by LDA was set at a distance of 360 mm from the front edge of the lower layer at a site downstream and the measuring volumes of LDA were located at a distance of 15.5, 23, 38, and 50 mm from the flume bed. However, the data at 50 mm are omitted because they overlap with the top data in Fig. 10. The Doppler signals measured at these points were recorded on tape with the signals of the interface displacements which were measured at a distance of 290 mm from the measuring position of LDA in the downstream direction. The determined relation between a velocity fluctuation in the principal flow and a generation of SVA was found through observation of the phenomena reproduced on a VTR. It can be seen in Fig. 10 that the wave packet is generated about 10 seconds after the shear above the interface reaches the highest value ; the approach of the data at 23 mm and that of 38 mm shows the acceleration of the shear layer above the interface. The time difference is reasonable if we take into consideration the following ; the distance between the measuring position of the velocity and that of the interface displacement and the mean velocity of principal flow. In Fig. 11, the time series of the transfigurement of the velocity profile from

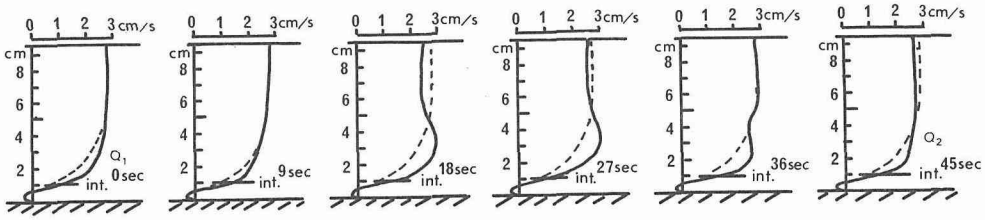

Fig. 11 Time series of the instantaneous velocity profile.

the time at point P_0 to the time at point P_3 is followed every 9 sec. The transfigurement of the time line due to the large scale vortex is shown in Fig. 12. The right end and the left end of the pattern in Fig. 12 correspond in time to the points P_1 and P_2 in Fig. 10. The increase of the shear just above the interface due to the vortex can be seen in Fig. 12 as well as Fig. 11. The stability of the shear layer can be examined by using these data and the linear stability theory.

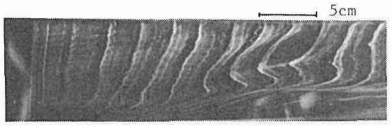

Fig. 12 Transfigurement of the time lines.

4. Procedure of numerical analysis based on the stability theory

We approximate the actual velocity distribution to a hyperbolic tangent profile as shown in Fig. 13, i. e.

$$U^* = V \tanh Y^*/l \tag{1}$$

where l, V, y^*, and U* are the characteristic length, the characteristic velocity, the vertical coordinate and the horizontal velocity. The asterisk means the dimensional variable. The amplitude, ϕ, of nondimensional stream function for small perturbations in the two-layer flow satisfies the Orr-Sommerfeld equations

$$(U-C)(\phi_1''-\alpha^2\phi_1)-U''\phi_1=\frac{1}{i\alpha R_e}(\phi_1^{IV}-2\alpha^2\phi_1''+\alpha^4\phi_1) \tag{2}$$

$$(U-C)(\phi_2''-\alpha^2\phi_2)-U''\phi_2=\frac{1}{i\alpha R_e}(\phi_2^{IV}-2\alpha^2\phi_2''+\alpha^4\phi_2) \tag{3}$$

with the boundary condition

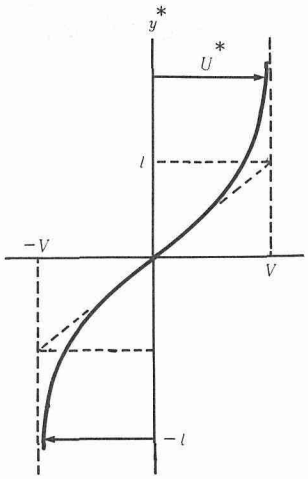

Fig. 13 Model of velocity profile and definition of the characteristic values.

$$\phi_1=\phi_1'=0 \qquad (y=+\infty) \tag{4}$$

$$\phi_2=\phi_2'=0 \qquad (y=-\infty) \tag{5}$$

$$\phi_1=\phi_2 \qquad (y=0) \tag{6}$$

$$\phi_1'-\frac{U'}{(U-C)}\phi_1=\phi_2'-\frac{U'}{(U-C)}\phi_2 \qquad (y=0) \tag{7}$$

$$\gamma\phi_1''-\gamma\left\{\frac{U''}{(U-C)}-\alpha^2\right\}\phi_1=\phi_2''-\left\{\frac{U''}{(U-C)}-\alpha^2\right\}\phi_2 \qquad (y=0) \tag{8}$$

$$i\gamma\phi_1'''+\gamma\alpha\{R_e(U-C)-3i\alpha\}\phi_1'-\gamma\alpha R_e U'\phi_1=i\phi_2'''+\alpha\{R_e(U-C)-3i\alpha\}\phi_2'-\alpha R_e U'\phi_2$$

$$-\frac{R_i R_e}{(U-C)}\phi_2 \qquad (y=0) \tag{9}$$

where the primes denote the differential coefficient, U the horizontal velocity, c the phase velocity, g the acceleraion of gravity, y the vertical coordinate, α the wave number, $R_e=lV/$

ν, $R_i=(1-\gamma)gl/V$, $\gamma=\rho_1/\rho_2$, ν the kinematic viscosity of the lower layer or upper layer, ρ the density and subscripts 1 and 2 indicate fresh water and saline water. The eigenvalue equation for our flow system is then

$$|\Delta(\alpha, C, R_e, R_i)|=0 \tag{10}$$

By using the numerical solutions of the O-S equation and equation (10), we can obtain α, R_e, and R_i values of growthable disturbances.

5. Discussion

Nishida and Yoshida obtained the neutral curves for several R_e values through the numerical integration following the Runge-Kutta-Gill procedure. One of their essential results is described in Fig. 14 which shows the distribution of the amplitude and the stream lines near the interface, which was not found in the Hazel's numerical investigation. This result indicates that the displacement of the stream lines has a maximum amplitude at the critical level just above or beneath the interface. Thus, the possibility of SVA and SVB growths is also confirmed by the linear instability theory. However, we investigated the qualitative agreement between the results of the experiment and the theory in order to conclude the SVA and SVB problem. Fig. 15 shows the initial stage wave numbers and the phase velocities of SVA obtained through experimental and the theoretical analysis. Since the initial stage wave number should be the most unstable, the agreement between the observed and numerical values in Fig. 15 is evident. The author has not yet finished

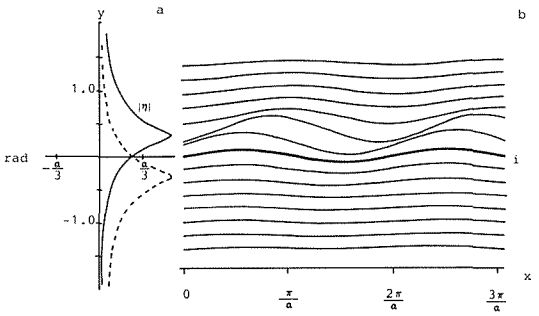

Fig. 14 (a) distributions of wave displacement amplitude $|\eta|$ $(=-\phi'/(U-C))$——: the amplitude for positive C_r (real part of C). ------: the amplitude of symmetric wave. (b) stream lines of unstable flow only for positive C_r case. i : interface.

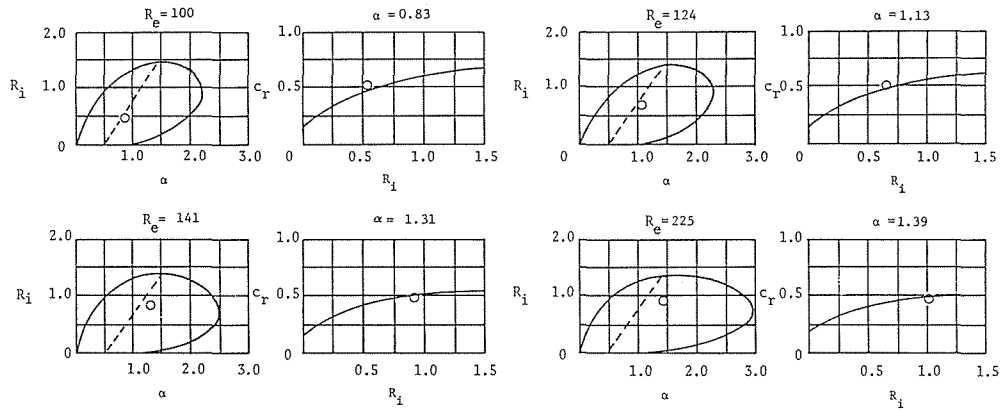

Fig. 15 Experimental α and C_r values at the initial stage of SVA growth.——: theoretical result of neutral curve or C_r.------: the most unstable wave number. ○ : experimental value

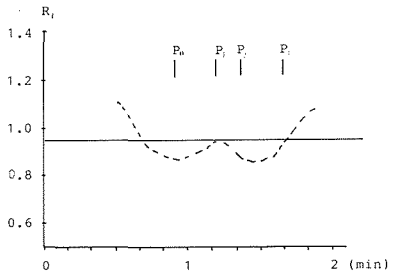

Fig. 16 Time series of R_i.——: theoretical result. ------: experimental result.

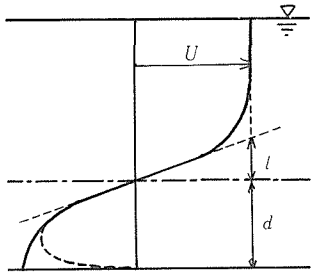

Fig. 17 Velocity distribution and its model profile near the lower layer front.

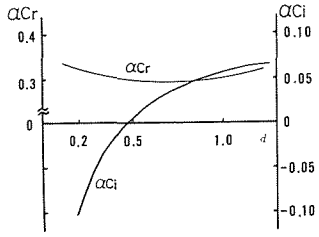

Fig. 18 Growth rate of SVA at initial stage. αC_r: phase velocity. αC_i : growth rate. d : lower layer depth divided by l.

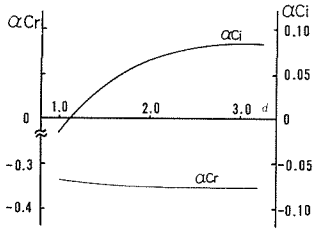

Fig. 19 Growth rate of SVB at initial stage. αC_r: phase velocity. αC_i : growth rate. d : lower layer depth divided by l.

examining the SVB property. However, we can at least conclude that SVA generates through the internal shear instability.

The shear instability of the two-layer flow during the large scale vortex transit can be examined in the same way. If the shear instability can be ascertained only in the time interval during which the interfacial wave packet generates, the purpose of this research will be achieved. The broken line in Fig. 16 shows the time series of R_i obtained by using the velocity profiles for the time between P_0 and P_3 with in Fig. 10. In the figure, the solid line is the critical R_i which is calculated using the tanh profiles fitting in well with the actual velocity near the interface. The result shows that the experimental data corresponding to P_0 P_3 intervals in Fig. 10 are lower than the numerical values. These results are sufficient to conclude that the interfacial wave packet is due to SVA growth, and the latter generates through the shear instability.

Lastly, we indicate that SVB does not occur at the interface near the lower layer front. A velocity distribution near the front is described in Fig. 17 with a model profile. The model profile is a tanh curve having an inflection point coinciding with the density interface. Therefore, the model profile is essentially antisymmetric. For this profile, numerical growth rates are given by the solid lines in Figs. 18 and 19. From these figures, we can see the critical depth for SVA and SVB growth. The result shows that the small depth of the lower layer forces the lower layer flow tends to stabilize ; as a result, SVA occurs individually at the interface near the front.

6. Conclusions

The growing process of the interfacial wave packet is summarized in the following four stages :

1) Occurrence of longitudinal vortices in internal shear layer.
2) The large scale vortex growth, out of the longitudinal vortices.
3) Generation of the coherent vortices, SVA and SVB, beneath the large scale vortex.
4) The growth of the interfacial wave packet due to the coherent vortices.

In this process, the growth mechanism of SVA packet at the interface near the lower layer front is clarified with the numerical analysis based on the linear stability theory. Individual occurrence of SVA near the front is caused by the stabilization of the flow in the small depth lower layers.

Acknowledgment

This research was partly supported by Scientific Research Grant of the Education Ministry under Thesis No. 59350034.

References

1) Helmholtz, H. : Phil. Mag. 36 (1868), 4, p. 337-346
2) Kelvin, W. : Phil. Mag. 42 (1871), 4, p. 368-374
3) Thorpe, S. A. : JFM, 46 (1971), p. 299-319
4) Keulegan, G. H. : J. Research, Nat., Bureau Stands., 43 (1949), p. 487-500
5) Holmboe, J. : Geofys. Publ., 24 (1962), 2, p. 67-113
6) Hazel, P. : JFM, 51 (1972), 1, p. 39-61
7) Yoshida, S. : Coast. Eng. Japan, 20 (1977), p. 7-15
8) Yoshida, S. : Proc. 2nd Int. Sympo. Stratified Flows, (1980), 2, p. 1062-1073
9) Tashiro, Y., S. Yoshida and M. Yoneya : Proc. 27th Japanese Conf. Hydraulics, (1983), p. 523-530
10) Hino, M., N. S. Hung and M. Hasegawa : Proc. 27th Japanese Conf. Hydraulics, (1983), p. 531-535
11) Nishida, S. and S. Yoshida : Theoretical and Applied Mech., 32 (1984), p. 35-45